Received 31 March 2023; revised 5 June 2023; accepted 1 July 2023. Date of publication 11 July 2023; date of current version 19 December 2023.
The review of this article was arranged by Editor H. Ma.

Digital Object Identifier 10.1109/JEDS.2023.3294439

Study on Amorphous InGaZnO Thin-Film Transistor Modeling Method Based on Artificial Neural Network

YINGTAO XIE[1] (Member, IEEE), KUNLIN CAI[1] (Member, IEEE), HUAN JIAN[1], YANLIN HUANG[1], JIAMING WENG[2] (Member, IEEE), AND WEI WANG[1] (Member, IEEE)

1 Department of Electronic Engineering, Chongqing University of Posts and Telecommunications, Chongqing 400065, China
2 Department of Electrical Engineering, Shanghai Jiao Tong University, Shanghai 200240, China

CORRESPONDING AUTHOR: Y. XIE (e-mail: xieyt@cqupt.edu.cn)

This work was supported in part by the National Natural Science Foundation of China under Grant 61804019; in part by the Science and Technology Research Program of Chongqing Municipal Education Commission under Grant KJZD-K202200607; and in part by the Chongqing Postgraduate Research and Innovation Project under Grant CYS22441.

ABSTRACT In this work, two approaches of forward design neural network and reverse design neural network were proposed to accelerate the design of passivation-layer structured amorphous indium gallium zinc oxide thin-film transistor (a-IGZO TFT). It was based on a neural network with the back-propagation neural network (BPNN) and general regression neural network (GRNN) as general approximators. The forward design neural network utilized the density-of-states (DOS) key parameters of a-IGZO film as input signals, and could quickly predict characteristic curves with high accuracy. The forward design effectively improved the problem of complex input/output layer parameters in the existing methods, which was significant for the prediction and optimization of a-IGZO TFT device performance. And the reverse design neural network adopts the DOS key parameters of a-IGZO film as the output signal to achieve the rapid prediction of DOS parameters of a-IGZO film. The inverse design effectively compensated the drawback that a-IGZO TFT required artificial tuning of DOS key parameters to achieve characteristic curve fitting. All in all, the neural network model can effectively determine whether the output parameters of the network meet the design objectives and whether the output parameters need to be changed by adjusting the input parameters to eventually achieve the performance prediction and material parameters optimization of a-IGZO TFT.

INDEX TERMS a-IGZO TFT, density-of-states, reverse design neural network, radio-frequency power.

I. INTRODUCTION

With the development of wearable devices, artificial intelligence, and the Internet of things, the industry is looking forward to integrated circuit designs based on a thin-film transistor (TFT) with low latency, low power consumption, and high stability. Among them, the amorphous indium gallium zinc oxide thin-film transistor (a-IGZO TFT) has attracted much attention because of its high mobility, simple preparation process, low cost, and good uniformity [1], [2], [3], [4]. The a-IGZO TFT is very suitable for the large-scale circuit on board and has been successfully applied in various directions, such as pixel circuits [5], logic circuits [6], radio-frequency (RF) identification [7], wearable flexible integrated devices [8], and flexible displays [9]. In addition, since external factors such as water vapor and oxygen can directly affect the performance of a-IGZO TFT, depositing SiO_x passivation-layer above the channel by RF sputtering can effectively block the corrosive medium from penetrating the back-channel surface and enhance the stability of the device [10], [11]. Meanwhile, to investigate the electrical properties of a-IGZO TFT, modeling from the density-of-states (DOS) properties of a-IGZO thin-film is a feasible approach [12], [13]. The DOS is an important concept in the amorphous semiconductor thin-film, which is used to represent the number of quantum states near a certain position in the energy band of a semiconductor material.

Moreover, the DOS combined with the Fermi-Dirac distribution can estimate the number of effective carriers of the material, which is important for the simulation.

The current research on a-IGZO TFT is mainly focused on the following aspects: adopting semiconductor layer doping process to improve device performance and stability [14], adopting new protective layer materials to improve device stability [15], developing new electrode materials [16], investigating the mechanism of device electrical stability [17], adjusting device structure and device applications [18], [19]. Among them, for the simulation of a-IGZO TFT device performance, the traditional physics-based modeling method is mainly done by modeling the device and scanning the corresponding physical quantity parameters by TCAD simulation software, but the method is very time-consuming and tedious, and it is difficult to keep up with the development of a-IGZO TFT. The rapid development of the neural network, on the other hand, provides an alternative for fast device and material prediction, which can reduce computational costs and shorten the development cycle while ensuring accuracy. For example, the back-propagation neural network (BPNN) was proposed by Rumelhart's group in 1986 [20], which consists of two processes in the learning process: forward propagation of the signal and back-propagation of the error. the BPNN has a strong nonlinear mapping capability and is one of the most widely used neural network models [21]. Similarly, the general regression neural network (GRNN) was proposed by Specht in 1991 based on the nonlinear regression theory [22]. The GRNN has a better network adaptation capability, which makes the neural network more convenient for network training and learning [23]. Hence, the artificial neural network (ANN) as a data-oriented modeling approach can be a very good alternative for modeling semiconductor devices if detailed device physics is not involved. Unfortunately, the neural network model applicable to a-IGZO TFT with the passivated-layer structure has not been reported.

Since the RF power of passivation-layer deposition had a significant impact on the device performance of a-IGZO TFT, this work proposed an ANN-based modeling approach for a-IGZO TFT performance prediction and structure optimization. After simulating the device performance under various RF powers based on DOS key parameters, a large amount of data from simulation calculations was collected for learning and training, and the two functions were executed according to the different requirements of BPNN and GRNN. The forward design approach predicted transfer characteristic curves and output characteristic curves of a-IGZO TFT device by using the device structure information (e.g., DOS key parameters, gate-source voltage, source-drain current, etc.). The reverse design approach was used to predict the DOS key parameters of a-IGZO TFT by using transfer characteristic curves of the device. The results demonstrated that the output can be obtained quickly based on the given input and the discrepancy between experimental, simulated, and predicted data can be compared directly, thus improving the efficiency of the a-IGZO TFT design process. In a word, this work was aimed at solving the bottleneck problem of a-IGZO TFT device modeling and constructing an a-IGZO TFT neural network model with reliable, high accuracy, and good generalization.

II. ARTIFICIAL NEURAL NETWORK APPROACH

The artificial neural network (ANN) does not depend on the model control method, and it has a strong adaptive capability, learning capability, and nonlinear mapping capability, which can optimize the network composition according to external data. Consequently, this work selected the back-propagation neural network (BPNN) and the general regression neural network (GRNN) to establish a-IGZO TFT neural network model for device performance prediction and structure optimization. This section introduced the theory related to BPNN and GRNN, and the regression evaluation index of the neural network.

A. THEORETICAL OVERVIEW OF BPNN AND GRNN

The most significant advantage of BPNN is that it can find an optimal prediction law by adjusting the weight coefficients through its learning algorithm, which gives it the ability to approximate arbitrary nonlinear functions [24]. The error back-propagation learning algorithm, or BP algorithm, is generally referred to as a three-layer feedforward network because it contains a three-layer network structure, as shown in Fig. 1 (a). The difference with BPNN is that GRNN is utilizing activation neurons to approximate the function, which has strong nonlinear mapping ability and learning speed. Moreover, GRNN not only has a strong advantage in approximating functions but also has a certain amount of fault tolerance and robustness [25]. When the sample data is limited, GRNN has a great prediction effect and is suitable for dealing with unstable data. GRNN has a four-layer structure, which are the input layer, pattern layer, summation layer, and output layer, as shown in Fig. 1 (b).

B. REGRESSION EVALUATION INDEXES OF THE NEURAL NETWORK

When the neural network is over-training, the trained model is applied to the test set for testing. The error between the predicted and actual values of the model on the test set is compared to determine the regression ability of the model and to determine whether it is necessary to return to the model constructing stage to modify the network structure. This is repeated until the performance on the test set reaches the expected goal. In particular, regression evaluation indexes of the neural network are Mean absolute error (MAE), Mean relative error (MRE), Mean squared error (MSE), and Coefficient of determination (R^2) [26], [27], as shown in Equation (1) to Equation (5).

$$\mathrm{MAE}(y, \widehat{y}) = \frac{1}{n}\sum_{i=1}^{n}|(y_i - \widehat{y_i})| \tag{1}$$

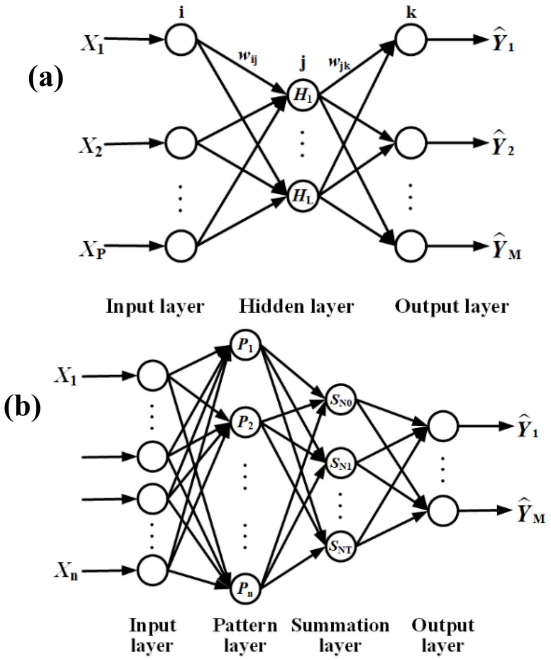

FIGURE 1. The structure of (a) BPNN (b) GRNN.

$$\mathrm{MRE}(y,\hat{y}) = \frac{1}{n}\sum_{i=1}^{n}\left|\frac{y_i-\hat{y}_i}{y_i}\right| \times 100\% \quad (2)$$

$$\mathrm{MSE}(y,\hat{y}) = \frac{1}{n}\sum_{i=1}^{n}(y_i-\hat{y}_i)^2 \quad (3)$$

$$R^2(y,\hat{y}) = 1-\frac{SS_{\mathrm{residual}}}{SS_{\mathrm{total}}} = 1-\frac{\sum_{i=1}^{n}(y_i-\hat{y}_i)^2}{\sum_{i=1}^{n}(y_i-\bar{y}_i)^2} \quad (4)$$

$$\bar{y} = \frac{1}{n}\sum_{i=1}^{n}y_i \quad (5)$$

where y_i is the predicted value of the i-th sample, $\hat{y}_i$ is the actual value of the i-th sample, $\bar{y}$ is the mean of the predicted values of the samples, n is the total number of samples, SS_{residual} denotes the square sum of the residuals, and SS_{total} denotes the square sum of the residuals where the predicted values are all $\bar{y}$.

III. EXPERIMENTAL

This work was divided into four steps: fabrication of a-IGZO TFT device, TCAD simulation based on DOS key parameters, forward and reverse design of the neural network, and performance prediction and structure optimization of the device. Critically, a large amount of data calculated based on DOS key parameters simulation were used as the dataset for the neural network. Only by selecting a well-characterized dataset, a neural network model of a-IGZO TFT could be developed to meet the expectations. This section introduced the previous three steps.

A. FABRICATION OF a-IGZO TFT DEVICE

Fig. 2 presents a cross-sectional diagram of the fabricated a-IGZO TFT device. At first, a 140/3300 Å Mo/Cu gate electrode layer was deposited on a cleaned glass substrate by a physical vapor deposition (PVD) process, and the corresponding pattern was prepared by a standard photolithography process. The next step was the preparation of 300/2000 Å SiN_x/TEOS_SiO_x (Tetraethyl orthosilicate, abbreviated as "TEOS") gate insulation layer based on a plasma-enhanced chemical vapor deposition (PECVD) process. Subsequently, the 600 Å a-IGZO (In: Ga: Zn = 1: 1: 1) semiconductor layer was sputtered by a PVD process. a-IGZO semiconductor layer was annealed in compressed dry air at 350 °C for 1 hour, and its patterning was obtained by standard photolithography and glycolic acid wet lithography techniques. A PVD process was performed on the patterned a-IGZO semiconductor film to sputter 140/3300 Å Mo/Cu layers, followed by a degumming process to obtain source/drain patterned electrodes, which was the back-channel etch (BCE) method. At last, the SiO_x passivation-layer was deposited by a PECVD process, in which the RF power was chosen to 600 W, 1000 W, and 1400 W, respectively, and then samples were annealed in the oven for 1 hour. In this case, the channel width to length ratio *W/L* of the device was 10/10 μm.

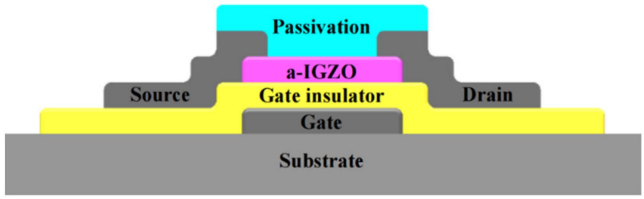

FIGURE 2. A cross-sectional diagram of the fabricated a-IGZO TFT device.

B. TCAD SIMULATION BASED ON DOS KEY PARAMETERS (CREATION OF THE DATASET)

Based on the fabricated a-IGZO TFT device, it was important to create a valuable dataset to establish the a-IGZO TFT neural network model that met the expectations. The DOS in the a-IGZO semiconductor layer determined the electrical characteristics and stability of the device to a large extent, and it was able to reveal the physical mechanism of the influence of the process on the device performance during the preparation process. Accordingly, a high concentration of doping on both sides of the a-IGZO layer (the doping level was 10^{20} cm^{-3}) was selected to simulate the repair effect of SiO_x passivation-layer deposition on the a-IGZO channel. Meanwhile, to collect a sufficient dataset, the a-IGZO TFT device was simulated by TCAD software based on DOS key parameters, and the values of six key parameters, including the density of the conduction band tail states (*NTA*), the characteristic decay energy of acceptor-like tail states (*WTA*), the density of the Gaussian acceptor-like states (*NGA*), the density of the Gaussian donor-like states (*NGD*), the energy corresponding to the peak for acceptor-like Gaussian states (*EGA*), and the energy corresponding to the peak for donor-like Gaussian states (*EGD*), were varied to simulate transfer

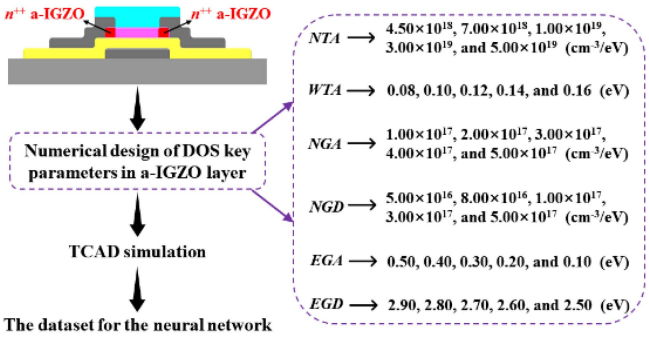

FIGURE 3. The process of creating the neural network dataset.

characteristic curves and output characteristic curves of the device one by one. The flow chart for creating the dataset was shown in Fig. 3.

The values of *NTA* were selected as 4.50×10^{18}, 7.00×10^{18}, 1.00×10^{19}, 3.00×10^{19}, and 5.00×10^{19} cm^{-3}/eV, respectively. The values of *WTA* were selected as 0.08, 0.10, 0.12, 0.14, and 0.16 eV, respectively. The values of *NGA* were selected as 1.00×10^{17}, 2.00×10^{17}, 3.00×10^{17}, 4.00×10^{17}, and 5.00×10^{17} cm^{-3}/eV, respectively. The values of *NGD* were selected as 5.00×10^{16}, 8.00×10^{16}, 1.00×10^{17}, 3.00×10^{17}, and 5.00×10^{17} cm^{-3}/eV, respectively. The values of *EGA* were selected as 0.50, 0.40, 0.30, 0.20, and 0.10 eV, respectively. The values of *EGD* were selected as 2.90, 2.80, 2.70, 2.60, and 2.50 eV, respectively. It should be emphasized that in the dataset, since *NTA*, *NGA*, *NGD* and drain-source current (I_{ds}) contained orders of magnitude, these four data required logarithmic processing before they could be utilized in the training of the neural network. In particular, when transfer characteristic curves were simulated, the values of the gate-source voltage (V_{gs}) were selected as 25.0, 24.5, 24.0, $\cdots$, 0.5, and 0 V, respectively, and the value of the drain-source voltage (V_{ds}) was 10 V. When output characteristic curves were simulated, the values of the V_{ds} were selected as 25.0, 24.5, 24.0$\cdots$ 0.5, and 0 V, respectively, and the values of the V_{gs} were selected as 0, 5, 10, 15, 20, and 25 V, respectively.

C. FORWARD AND REVERSE DESIGN OF THE NEURAL NETWORK

C.1. FORWARD DESIGN NEURAL NETWORK

The purpose of the forward design was to predict the electrical characteristics based on the DOS key parameters (e.g., *NTA*, *WTA*, *NGA*, *NGD*, *EGA*, and *EGD*) of the device using BPNN and GRNN, respectively. The forward design allowed for rapid verification of the device design and thus the optimization of the device.

Fig. 4 presents the topological structure of the proposed forward design neural network. It could be seen that two different topological structures were designed due to the requirement to predict transfer characteristic curves and output characteristic curves of the a-IGZO TFT device. It was particularly important to note that BPNN and GRNN had the

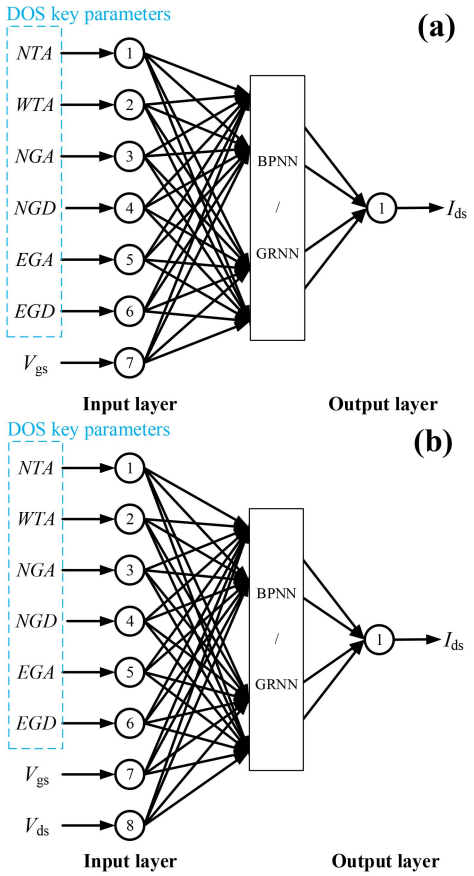

FIGURE 4. The topological structure of the proposed forward design neural network to predict (a) transfer characteristic curves (b) output characteristic curves.

same input parameters and output parameters when establishing the topologies, although the network structures of the middle part of both were different. For the prediction of transfer characteristic curves, the DOS key parameters of a-IGZO thin-film and V_{gs} were selected as the input parameters of the forward design neural network, and I_{ds} was selected as the output parameter. It means that seven input signals and one output signal were required to predict transfer characteristic curves. For the prediction of output characteristic curves, the DOS key parameters, V_{gs} and V_{ds} were adopted as the input parameters of the inverse design neural network, and I_{ds} was adopted as the output parameter. In other words, eight input signals and one output signal were employed to predict output characteristic curves.

C.2. REVERSE DESIGN NEURAL NETWORK

In response to the traditional method of TFT design that required a tedious optimization process of physical modeling and parameter scanning, this work creatively proposed a reverse design neural network. The reverse design method in this work was complemented by the forward design method, and the input and output variables of both were opposite.

The reverse design neural network was developed to predict the DOS key parameters from transfer characteristic

TABLE 1. Comparison of regression evaluation indexes for transfer characteristic curves predicted by BPNN and GRNN with various RF powers.

Type	RF power (W)	Optimal node	Optimal spread	Regression evaluation indexes			
				MSE	MAE	MRE	R^2
BPNN	600	6		0.012	0.074	1.141%	0.998
	1000	11		0.130	0.231	2.493%	0.990
	1400	10		0.071	0.172	2.062%	0.992
GRNN	600		0.059	0.058	0.112	1.493%	0.987
	1000		0.066	0.069	0.178	2.729%	0.981
	1400		0.052	0.187	0.213	3.754%	0.977

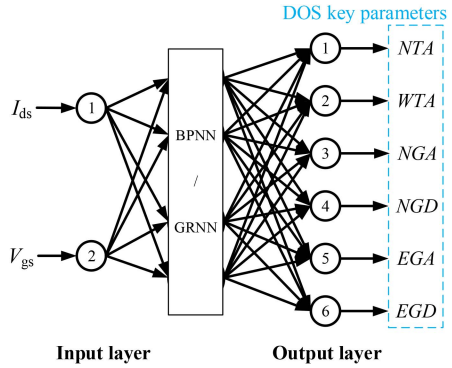

FIGURE 5. The topological structure of the proposed reverse design neural network to predict the DOS key parameters.

curves of a-IGZO TFT device, which could be applied to meet the design requirements of different devices in practical situations. Fig. 5 presents the topological structure of the proposed reverse design neural network. In this regard, V_{gs} and I_{ds} were selected as the input parameters of the inverse design neural network, and the DOS key parameters were selected as the output parameters. In other words, two input signals and six output signals were required to predict the DOS key parameters of the a-IGZO thin-film.

IV. RESULTS AND DISCUSSION

A. RESULTS OF THE FORWARD DESIGN NEURAL NETWORK

Combining the neural network with the huge dataset of TCAD simulation calculations. For the prediction problem of a-IGZO TFT device performance at various RF powers, the optimized BPNN algorithm and GRNN algorithm were used to achieve the prediction of characteristic curves, respectively. It should be noted that the same values of the DOS key parameters were used when predicting transfer characteristic curves and output characteristic curves. Fig. 7 presents the predicted transfer characteristic curves of a-IGZO TFT at 600 W, 1000 W, and 1400 W RF power by the forward design neural network (without considering the cutoff region), respectively. It was observed that the predicted transfer characteristic curves based on BPNN and GRNN in both linear and semi-logarithmic coordinates were fitted with the experimental and simulated data, which verified the feasibility of the proposed forward-designed neural network. In addition, BPNN had a better ability to predict transfer characteristic curves compared with GRNN, and the errors between predicted data and experimental data were smaller. The results demonstrate that the outputs could be obtained quickly based on the given inputs and the differences between experimental, simulated, and predicted data could be compared directly, thereby improving the efficiency of the a-IGZO TFT design process.

After the forward design neural network predicted transfer characteristic curves, to compare the prediction effects of BPNN and GRNN, the regression evaluation indexes calculated by Equation (2) to Equation (5) were shown in TABLE 1. For BPNN, the optimal node of the hidden layer at 600 W, 1000 W, and 1400 W RF power was determined by Equation (1) to be 6, 11, and 10, respectively. for GRNN, the optimal spread at 600 W, 1000 W, and 1400 W RF power was determined by the cross-validation method to be 0.059, 0.066, and 0.052, respectively. Furthermore, at 1000 W RF power, the results of MSE, MAE, MRE, and R^2 for BPNN were 0.130, 0.231, 2.493%, and 0.990, respectively, while the results of MSE, MAE, MRE, and R^2 for GRNN were 0.069, 0.178, 2.729%, and 0.981, respectively. The data of transfer characteristic curves and regression evaluation indexes were analyzed comprehensively. The results demonstrated that for the prediction of a single curve with the multiple inputs and single output, BPNN only required the adjustment of the optimal node in the hidden layer to achieve. Unfortunately, the approximation capability of GRNN was weakened due to a large amount of the sample data.

After predicting transfer characteristic curves, output characteristic curves were predicted based on the forward design neural network. Fig. 6 presents the predicted output characteristic curves of a-IGZO TFT at 600 W, 1000 W, and 1400 W RF power, respectively. The simulated data were not exhibited in Fig. 6 because of the well-fitting experimental and simulated data and a large number of curves. It was observed that output characteristic curves predicted based on BPNN had an ideal fit with the experimental data for the values of V_{gs} as 0 V, 5 V, 10 V, 15 V, 20 V, and 25 V, respectively, while the prediction results based on GRNN were worse. The potential reason was that predicting output characteristic curves required fitting six curves with large variability at the same time. The parameters to be adjusted by BPNN were the number of nodes in the hidden layer, the

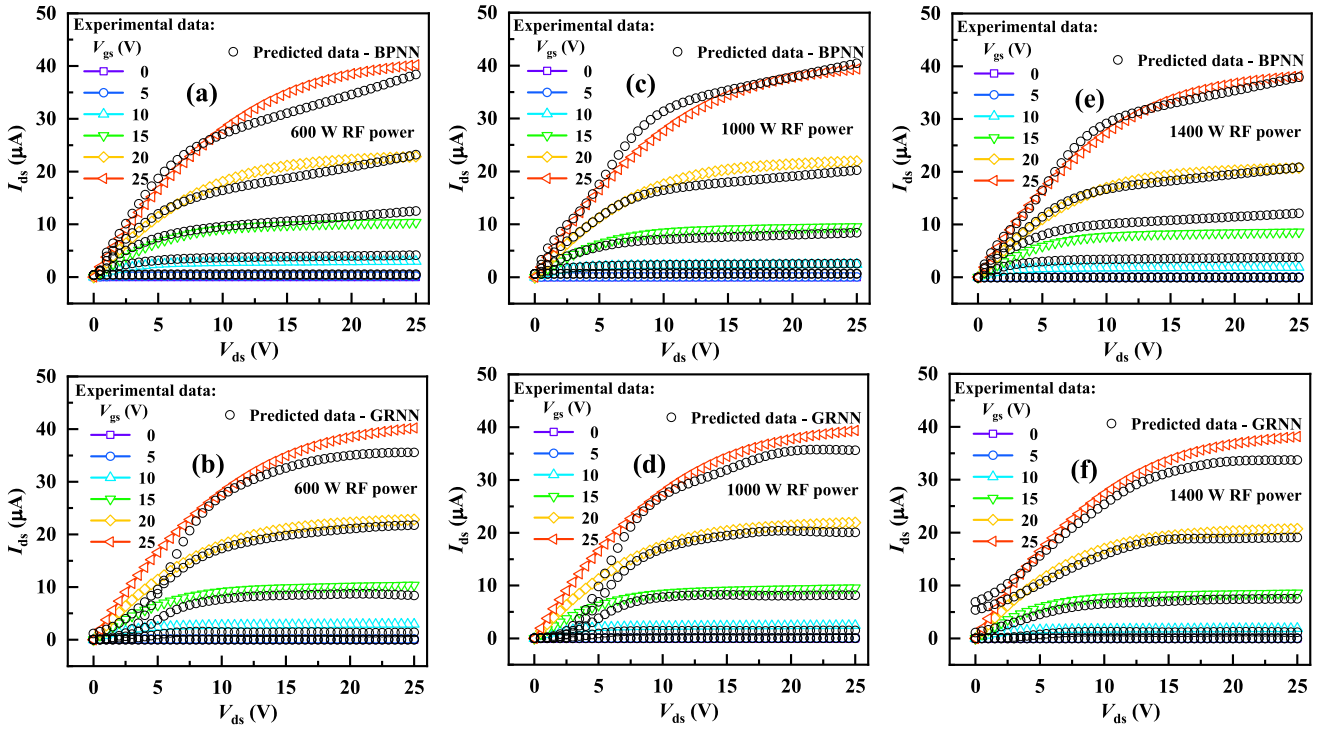

FIGURE 6. Data comparison of output characteristic curves predicted by forward design neural network. 600 W RF power (a) BPNN (b) GRNN; 1000 W RF power (c) BPNN (d) GRNN; 1400 W RF power (e) BPNN (f) GRNN.

TABLE 2. Comparison of regression evaluation indexes for output characteristic curves predicted by BPNN and GRNN with various RF powers.

Type	RF power (W)	Optimal node	Optimal spread	Regression evaluation indexes			
				MSE	MAE	MRE	R^2
BPNN	600	13		0.170	0.210	2.330%	0.985
	1000	13		0.038	0.137	1.888%	0.990
	1400	13		0.151	0.260	3.335%	0.985
GRNN	600		0.245	0.658	0.704	7.922%	0.891
	1000		0.259	0.573	0.654	7.963%	0.898
	1400		0.251	0.707	0.773	8.052%	0.882

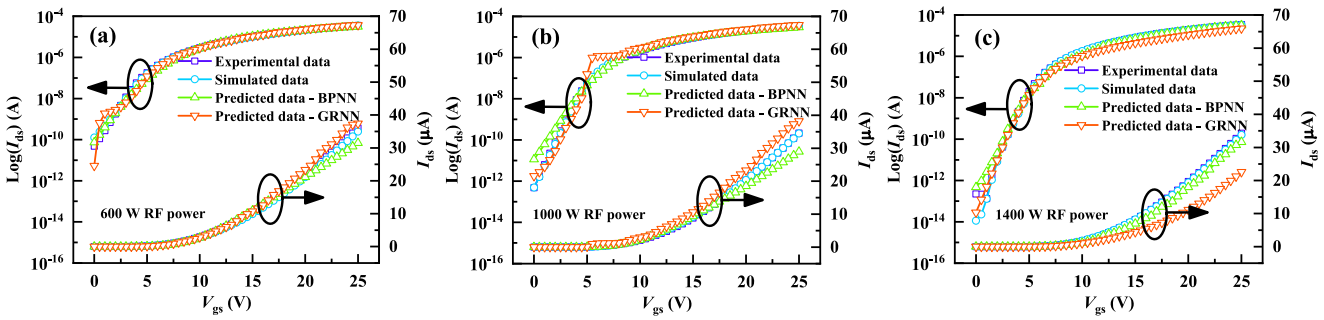

FIGURE 7. Data comparison of transfer characteristic curves predicted by forward design neural network (a) 600 W RF power (b) 1000 W RF power (c) 1400 W RF power.

number of iterations, the training function, and the learning rate. However, the parameters to be determined by GRNN were mainly the spread parameter.

Similarly, after output characteristic curves were predicted by the forward design neural network, the regression evaluation indexes calculated by equation to compare the prediction effects of BPNN and GRNN were shown in TABLE 2. It was found that the BPNN determined the optimal node of the hidden layer for 600 W, 1000 W, and 1400 W RF power as 13 by the equation, while the

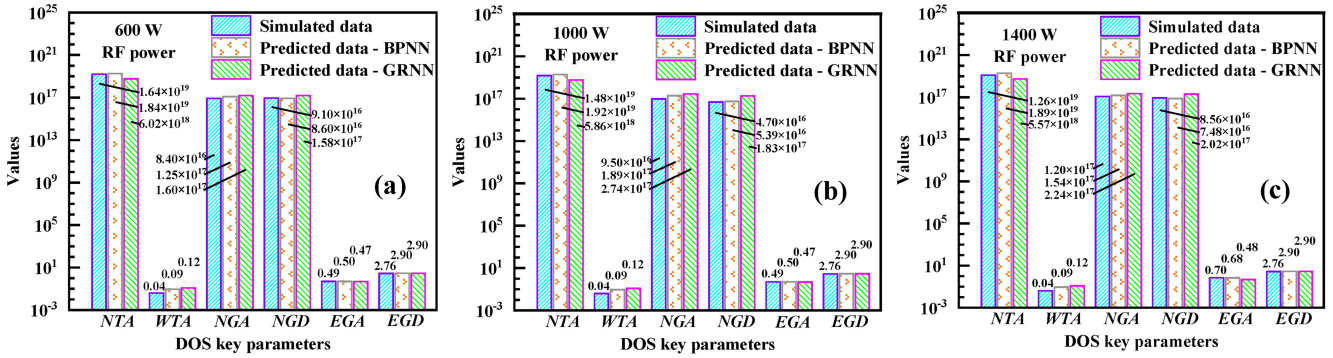

FIGURE 8. Data comparison of DOS key parameters predicted by reverse design neural network (a) 600 W RF power (b) 1000 W RF power (c) 1400 W RF power.

TABLE 3. Comparison of regression evaluation index for DOS key parameters predicted by BPNN and GRNN with various RF powers.

Type	RF power (W)	Optimal node	Optimal spread	Regression evaluation index (MRE)
BPNN	600	5		1.395%
	1000	12		1.143%
	1400	8		1.550%
GRNN	600		1	5.042%
	1000		1	5.828%
	1400		1	5.706%

GRNN determined the optimal spread for 600 W, 1000 W, and 1400 W RF power as 0.245, 0.259, and 0.251 by the cross-validation method, respectively. In addition, at 1000 W RF power, the results of regression evaluation indexes MSE, MAE, MRE, and R^2 for BPNN were 0.038, 0.137, 1.888%, and 0.990, respectively, while the results of regression evaluation indexes MSE, MAE, MRE, and R^2 for GRNN were 0.573, 0.654, 7.963%, and 0.898, respectively. Comprehensive analysis of the predicted data and regression evaluation indexes indicated that the ability of the BPNN to predict output characteristic curves was still favorable, the deviation of the predicted data from the experimental data was smaller, and the prediction of output characteristic curves was more accurate. It could be interpreted that although the smaller spread parameter of GRNN made the linear approximation ability of the function stronger, the too-small value of the spread parameter will lead to the function approximation curve not being smooth. Consequently, it caused the GRNN to have a better prediction in the saturation region and a worse prediction in the linear region.

B. RESULTS OF THE REVERSE DESIGN NEURAL NETWORK

The reverse design approach utilized transfer characteristic curves of the device to predict the DOS key parameters of the a-IGZO film. Fig. 8 presents the DOS key parameters predicted by the reverse design neural network at 600 W, 1000 W, and 1400 W RF power, respectively. It was observed that although the order of magnitude difference of the DOS key parameters was significant, the errors of the DOS key parameters predicted based on the BPNN were smaller than those predicted by the GRNN. For *NTA*, at 600 W RF power, the values of simulated data, BPNN data, and GRNN data were 1.64×10^{19} cm^{-3}/eV, 1.84×10^{19} cm^{-3}/eV, and 6.02×10^{18} cm^{-3}/eV, respectively. At 1000 W RF power, the values of simulated data, BPNN data, and GRNN data were 1.48×10^{19} cm^{-3}/eV, 1.92×10^{19} cm^{-3}/eV, and 5.86×10^{18} cm^{-3}/eV, respectively. At 1400 W RF power, the values of simulated data, BPNN data, and GRNN data were 1.26×10^{19} cm^{-3}/eV, 1.89×10^{19} cm^{-3}/eV, and 5.57×10^{18} cm^{-3}/eV, respectively. And for *EGA*, at 600 W RF power, the values of simulated data, BPNN data, and GRNN data were 0.49 eV, 0.50 eV, and 0.47 eV, respectively. At 1000 W RF power, the values of simulated data, BPNN data, and GRNN data were 0.49 eV, 0.50 eV, and 0.47 eV, respectively. At 1400 W RF power, the values of simulated data, BPNN data, and GRNN data were 0.70 eV, 0.68 eV, and 0.48 eV, respectively. The results validated the feasibility of the proposed reverse design neural network and revealed that reverse design enabled rapid prediction of material parameters.

After the reverse design neural network predicted the DOS key parameters, to compare the prediction effects of BPNN and GRNN, the regression evaluation index MRE calculated by equation was shown in TABLE 3. For the BPNN, the optimal node of the hidden layer at 600 W, 1000 W, and 1400 W RF power was determined to be 5, 12, and 8, respectively, and the regression evaluation index MRE at 600 W, 1000 W, and 1400 W RF power was calculated to be 1.395%, 1.143%, and 1.550%, respectively. For GRNN, the optimal spread of 1 for 600 W, 1000 W, and 1400 W RF power was determined by the cross-validation method, and the regression evaluation index MRE was calculated to be 5.042%, 5.828%, and 5.706% for 600 W, 1000 W, and 1400 W RF power, respectively. Comprehensive analysis of

the predicted data of DOS key parameters and the regression evaluation index indicated that compared with GRNN, BPNN had a better ability to predict DOS key parameters, and the error between the predicted data and the simulation data was smaller. It could be explicated that for the prediction of material parameters with the multiple inputs and multiple outputs, BPNN had the capability of approximating an arbitrary nonlinear function. In contrast, the large spread parameter of GRNN made the linear approximation ability of the function weaker, resulting in a slightly inferior prediction.

V. CONCLUSION

This work proposed the performance prediction and material parameters optimization of a-IGZO TFT with passivation-layer structure using the artificial neural network. The established neural network model was based on numerous simulations of the DOS of a-IGZO thin-film as the dataset. Subsequently, the BPNN and the GRNN were used to accelerate the design of a-IGZO TFT devices. In addition, the neural network model was designed with forward and reverse structures. Among them, the forward design neural network used the DOS key parameters as the input signal for device performance prediction, while the reverse design neural network used the DOS key parameters as the output signal for material parameters prediction. The results demonstrated that the proposed neural network model possessed ideal prediction results, and the BPNN was more accurate than GRNN in predicting device characteristic curves and DOS key parameters. The potential reason was that the parameters to be adjusted by BPNN were the number of nodes in the hidden layer, the number of iterations, the training function, and the learning rate. Meanwhile, the parameters to be determined by GRNN were mainly the spread parameter.

REFERENCES

[1] T. Kamiya, K. Nomura, and H. Hosono, "Present status of amorphous In-Ga-Zn-O thin-film transistors," *Sci. Technol. Adv. Mater.*, vol. 11, no. 4, Sep. 2010, Art. no. 044305, doi: 10.1088/1468-6996/11/4/044305.

[2] T. Kamiya and H. Hosono, "Material characteristics and applications of transparent amorphous oxide semiconductors," *NPG Asia Mater.*, vol. 2, pp. 15–22, Jan. 2010, doi: 10.1038/asiamat.2010.5.

[3] Y. T. Xie, D. P. Wang, and H. H. Fong, "High-performance solution-processed amorphous InGaZnO thin film transistors with a metal–organic decomposition method," *J. Nanomater.*, vol. 2018, May 2018, Art. no. 7423469, doi: 10.1155/2018/7423469.

[4] L. T. Zhang et al., "Source-drain resistance characteristics of back-channel etched amorphous InGaZnO thin film transistors with TiO_2: Nb protective layer," *Abbrev. Mater. Sci. Semicond. Process.*, vol. 68, pp. 147–151, Sep. 2017, doi: 10.1016/j.mssp.2017.04.020.

[5] C. W. Liao, "Mobility impact on compensation performance of AMOLED pixel circuit using IGZO TFTs," *J. Semicond.*, vol. 40, no. 2, Feb. 2019, Art. no. 22403, doi: 10.1088/1674-4926/40/2/022403.

[6] X. F. Xu, G. He, L. N. Wang, W. H. Wang, S. S. Jiang, and Z. B. Fang, "Optimization of electrical performance and stability of fully solution-driven α-InGaZnO thin-film transistors by graphene quantum dots," *J. Mater. Sci. Technol.*, vol. 141, pp. 100–109, Nov. 2022, doi: 10.1016/j.jmst.2022.09.016.

[7] S. K. Dargar and V. M. Srivastava, "Design of double-gate tri-active layer channel based IGZO thin-film transistor for improved performance of ultra-low-power RFID rectifier," *IEEE Access*, vol. 8, pp. 194652–194662, Oct. 2020, doi: 10.1109/ACCESS.2020.3034031.

[8] H. L. Ning et al., "Transparent flexible IGZO thin film transistors fabricated at room temperature," *Membranes*, vol. 12, no. 1, Dec. 2021, Art. no. 29, doi: 10.3390/membranes12010029.

[9] J. Y. Zhong et al., "Bilayer metal oxide channel thin film transistor with flat interface based on smooth transparent nanopaper substrate," *IEEE Electron Device Lett.*, vol. 43, no. 12, pp. 2113–2116, Dec. 2022, doi: 10.1109/LED.2022.3212071.

[10] J. C. Park, S. E. Ahn, and H. N. Lee, "High-performance low-cost back-channel-etch amorphous gallium–indium–zinc oxide thin-film transistors by curing and passivation of the damaged back channel," *ACS Appl. Mater. Interfaces*, vol. 5, no. 23, pp. 12262–12267, Nov. 2013, doi: 10.1021/am404490t.

[11] Y. T. Xie, K. L. Cai, P. L. Chen, H. Jian, J. M. Weng, and J. Y. Hu, "The effect of passivation-layer process to amorphous InGaZnO thin-film transistors using back-channel etch method," *Semicond. Sci. Technol.*, vol. 37, no. 4, Feb. 2022, Art. no. 45005, doi: 10.1088/1361-6641/ac46f7.

[12] C. E. Kim et al., "Density-of-states modeling of solution-processed InGaZnO thin-film transistors," *IEEE Electron Device Lett.*, vol. 31, no. 10, pp. 1131–1133, Sep. 2010, doi: 10.1109/LED.2010.2061832.

[13] H. Im et al., "Accurate defect density-of-state extraction based on back-channel surface potential measurement for solution-processed metal-oxide thin-film transistors," *IEEE Trans. Electron Devices*, vol. 64, no. 4, pp. 1683–1688, Apr. 2017, doi: 10.1109/TED.2017.2664661.

[14] A. Abliz et al., "Effects of nitrogen and hydrogen codoping on the electrical performance and reliability of InGaZnO thin-film transistors," *ACS Appl. Mater. Interfaces*, vol. 9, no. 12, pp. 10798–10804, Mar. 2017, doi: 10.1021/acsami.6b15275.

[15] S. H. Moon et al., "Combination of gate-stack process and cationic composition control for boosting the performance of thin-film transistors using In–Ga–Zn–O active channels prepared by atomic layer deposition," *ACS Appl. Electron. Mater.*, vol. 3, no. 11, pp. 4849–4858, Oct. 2021, doi: 10.1021/acsaelm.1c00689.

[16] Y. Kim, K. H. Lee, G. Mun, K. Park, and S. H. K. Park, "Outstanding performance as Cu top gate IGZO TFT with large trans-conductance coefficient by adopting double-layered Al_2O_3/SiN_x gate insulator," *Phys. Status Solidi A*, vol. 214, no. 12, Sep. 2017, Art. no. 1700183, doi: 10.1002/pssa.201700183.

[17] D. P. Wang, M. P. Hung, J. X. Jiang, T. Toda, C. Y. Li, and M. Furuta, "Effect of drain bias on negative gate bias and illumination stress induced degradation in amorphous InGaZnO thin-film transistors," *Jpn. J. Appl. Phys.*, vol. 53, no. 3S1, Jan. 2014, Art. no. 3CC01, doi: 10.7567/JJAP.53.03CC01.

[18] C. Y. Dong et al., "Improvements in passivation effect of amorphous InGaZnO thin film transistors," *Mater. Sci. Semicond. Process.*, vol. 20, pp. 7–11, Apr. 2014, doi: 10.1016/j.mssp.2013.12.009.

[19] C. Yuan, Y. Q. Li, X. H. Feng, and Z. D. Yuan, "Integrated gate driver circuit technology with IGZO TFT for AMOLED displays of simultaneous emission driving method," *J. Soc. Inf. Disp.*, vol. 52, no. S2, pp. 55–58, Aug. 2021, doi: 10.1002/sdtp.15019.

[20] D. E. Rumelhart, G. E. Hinton, and R. J. Williams, "Learning representations by back-propagating errors," *Nature*, vol. 323, pp. 533–536, Oct. 1986, doi: 10.1038/323533a0.

[21] C. S. Lin, J. Kuo, C. C. Lin, Y. L. Lay, and H. J. Shei, "Automatic inspection and strategy for surface defects in the PI coating process of TFT-LCD panels," *Assembly Autom.*, vol. 31, no. 3, pp. 244–250, Aug. 2011, doi: 10.1108/01445151111150587.

[22] D. F. Specht, "A general regression neural network," *IEEE Trans. Neural Netw.*, vol. 2, no. 6, pp. 568–576, Nov. 1991, doi: 10.1109/72.97934.

[23] F. Güneş, P. Mahouti, S. Demirel, M. A. Belen, and A. Uluslu, "Cost-effective GRNN-based modeling of microwave transistors with a reduced number of measurements," *Int. J. Numer. Model.*, vol. 30, nos. 3–4, Aug. 2015, Art. no. e2089, doi: 10.1002/jnm.2089.

[24] J. F. Xu and Z. Z. Liu, "A back propagation neural network-based algorithm for retrieving all-weather precipitable water vapor from MODIS NIR measurements," *IEEE Trans. Geosci. Remote Sens.*, vol. 60, Nov. 2022, Art. no. 5633614, doi: 10.1109/TGRS.2022.3219405.

[25] L. Zhang, Z. H. Xue, Y. J. Zhang, J. Y. Ma, and H. Li, "Enhanced generalized regression neural network for soil moisture estimation over the Qinghai-Tibet plateau," *IEEE J. Sel. Topics Appl. Earth Observ. in Remote Sens.*, vol. 15, pp. 3815–3829, Apr. 2022, doi: 10.1109/JSTARS.2022.3166978.
[26] G. Wang et al., "Optimization and performance prediction of tunnel field-effect transistors based on deep learning," *Adv. Mater. Technol.*, vol. 7, no. 5, Nov. 2021, Art. no. 2100682, doi: 10.1002/admt.202100682.
[27] Q. Y. Luo, J. X. Li, and H. Zhang, "Drag coefficient modeling of heterogeneous connected platooning vehicles via BP neural network and PSO algorithm," *Neurocomputing*, vol. 484, pp. 117–127, May 2022, doi: 10.1016/j.neucom.2020.12.136.

YINGTAO XIE (Member, IEEE) received the Ph.D. degree in electronic engineering from Shanghai Jiao Tong University, Shanghai, China, in 2015.

From 2016 to 2018, he was an Assistant Professor. He has been an Associate Professor with Electronic Engineering Department, Chongqing University of Posts and Telecommunications, China, since 2018. His research is in the area of metal oxide and organic electronics. This term refers to the use of metal oxide, organic, and other new materials to create electronic devices and driver circuit with unique capabilities.

KUNLIN CAI (Member, IEEE) received the B.S. degree from Wuyi University, China, in 2020. He is currently pursuing the master's degree with the School of Optoelectronic Engineering, Chongqing University of Posts and Telecommunications, China.

His research interests include the thin-film materials and flexible thin-film transistor devices.

HUAN JIAN, photograph and biography not available at the time of publication.

YANLIN HUANG, photograph and biography not available at the time of publication.

JIAMING WENG, photograph and biography not available at the time of publication.

WEI WANG, photograph and biography not available at the time of publication.